JCBI
Journal of Computing & Biomedical Informatics
ISSN: 2710 - 1606
Volume 06 Issue 02
2024

Research Article
https://doi.org/10.56979/602/2024

AI-Powered Radiology: Enhancing Efficiency and Accuracy in Knee Osteoarthritis Diagnosis through Automated Bone Segmentation

Ayesha Kiran[1*], Zobia Suhail[1], Anila Amjad[2], Muhammad Asad Arshed[3], and Zainab Zafar[4]

[1]Faculty of Computing and Information Technology, Department of Computer Science, University of the Punjab, Lahore, Pakistan.
[2]Department of Computer Science, University of Engineering and Technology, Lahore 54890, Pakistan.
[3]School of Systems and Technology, University of Management and Technology, Lahore 54770, Pakistan.
[4]Department of Computer Science, Government College University, Lahore 54000, Pakistan.
[*]Corresponding Author: Ayesha Kiran. Email: ayeshakiran2617@gmail.com

Received: January 01, 2024 **Accepted:** February 05, 2024 **Published:** March 01, 2024

Abstract: A significant number of people experience a decline in their quality of life annually due to Knee Osteoarthritis, a debilitating joint condition. Clinicians commonly diagnose osteoarthritis by identifying potential joint space narrowing visible in knee X-ray images. As bone segmentation is crucial for accurate measurement of joint space width, this process require an automated solution in the form a U-Net model. This paper demonstrates a deep learning-driven method for automated joint detection and bone segmentation in knee radiographs, incorporating a U-Net model with VGG11 encoder. The proposed solution effectively detects and extracts joints from radiographic images. Additionally, it precisely segments bones, obtaining a segmentation mean Intersection over Union (IOU) score of 0.963. An algorithmic approach is introduced for measuring vertical distances to determine the joint space width between the femur and tibia bones. With an accuracy rate of 89%, the images are reliably classified as either normal or exhibiting osteoarthritis.

Keywords: U-Net; Segmentation; Knee Osteoarthritis; Joint Space Width; Severity Grading; Deep Learning; Artificial Intelligence.

1. Introduction

The gradual erosion of articular cartilage in Knee Osteoarthritis (KOA) leads to eventual joint dysfunction and severe pain [1, 2]. Knee Osteoarthritis (KOA) stands as one of the prevailing arthritis types, often aligning with aging and consequently impacting a substantial portion of the elderly population [3]. Prominent indicators of Osteoarthritis (OA) encompass pain, stiffness, and decreased mobility. Diagnosis by a clinician typically involves assessing these signs, examining knee X-rays and a knee-focused physical examination [4]. Considering their affordability compared to MRI scans, knee radiographs serve as a tool for clinicians to assess possible joint space narrowing, bone deformities, and the existence of osteophytes [5].

The current clinical diagnostic process involves classifying Osteoarthritis (OA) into one of the five Kellgren- Lawrence (KL) grades [6]. One of the major indicators of OA is the Joint Space Width (JSW) present between the femur and tibia bones. Since this grading relies on experience and can be subjective, automated solutions have used minimum JSW for determining the progression of OA. In previous work, a two-step solution has been proposed by most researchers which incorporates using a joint detector algorithm and a deep learning classifier for classifying the severity of the disease into KL grades. In contrast some researchers have adopted traditional image processing techniques which are primarily based on edge detection. Mengko et al., [7] introduced an automated method for osteoarthritis (OA) detection through the computation of cartilage Joint Space Width (JSW). The extraction process for the Region of Interest (ROI) involved template matching and comparison of similarity between regions. Edge detection filters were used to compute the bone boundaries. JSWs were compared with the standard minimum JSW of

normal knee to determine the presence of OA. Similar to this method, the JSW between bones was measured in [8], and in addition, it was successful in identifying the formation of osteophytes.

The region of cartilage between the femur and tibia bones was segmented using an active contour algorithm in [9]. Subsequently, a random forest classifier was trained on shape, texture, and statistical features which resulted in a classification accuracy of 87.92%. In an alternative study, knee arthritis classification relied on the utilization of both Self Organizing Map (SOM) and Gabor filter methodologies. This approach incorporated 16 GLCM features and yielded notable classification of 93.8% for KL-0, and 88.9% for KL-4 respectively [2].

A different template matching approach was applied in [10] which used 20 pre-selected images of joint centers for scanning over the radiographs to locate joints. Additionally, a weighted nearest neighbor classifier was trained utilizing a diverse set of features, namely: Chebyshev, **T**exture**,** Haralick**,** the first four moments and multiscale histograms. The model demonstrated effective classification capabilities, achieving an accuracy of 91.5% for categorizing minimal OA images and 80.4% for distinguishing moderate OA images.

The above methods use machine learning approaches that have been quite successful in achieving high classification accuracies for KL- 0 and KL-4 grades. However, they fail to show improved results for OA progression. Bone segmentation is a crucial step when dealing with radiographic images which allows researchers to propose specific segmentation methods. Patella bones were segmented from X-ray images using landmark data to create a shape model for the bones [11]. Similarly, in their study, the authors [12] employed the Active Shape Model (ASM), to extract the tibia and femur bones from knee radiographs. Initially introduced by Cootes in [13], the ASM entails a predefined shape approximating the structure to be identified within the target image. This model iteratively adapts its shape to effectively match the contours present in the target image.

Varying methods were employed in [14-19], for segmenting bone regions in radiographic images. It included different preprocessing steps for denoising and enhancing the images. This was followed by either finding the strong edges of the bones using an edge detection method or using active contour segmentation. Most of the above approaches are semiautomatic and rely on parameters. In addition, the edge detection filters fail to capture the 3D structure of the bones and often compute irrelevant edges. Moreover, the problem with edge detection filters is that their results are not consistent in low quality images and often detect unwanted edges.

Deep Learning models have shown a tremendous success in detecting OA in radiographs as they utilize features learnt from text, images and speech data. Some of the DL solutions for OA detection are described below. A Fully Convolutional Neural (FCN) network was utilized in [20] to extract the knee joints from bilateral radiographs. The network used binary segmentation masks for pixel-based classification. The network's output predictions were utilized for finding the countours of joints. For classification of OA, a CNN model was trained which classified the images with an accuracy of 60%. Similarly, [21] used a Siamese CNN for severity detection of OA which involved feeding patches extracted from the lateral and medial compartments of knee joints into the network, resulting in an average multiclass accuracy of 66.71%.

Different CNN models with minor adjustments have been employed for the severity classification of knee OA in [22-25]. P. Chen et al., [26] used a customized YOLOv2 whereas Wang et al., used YOLO for joint detection in X-ray images [27]. Both gait and image features were utilized for classifying KOA based on KL grades [28]. Most of the DL solutions explained above have focused more on the localization of joints in X-ray images rather than the automatic segmentation of the bones. In this paper, a U-Net model has been proposed that automatically segments the joints and bones from X-ray images. Subsequently, a distance measurement algorithm is developed to calculate the minimum JSW of the bones. And based on the computed JSW, the knee is classified as healthy or affected by OA. Previously, Cheung et al., accurately segmented femur and tibia bones using a U-Net model. However, it fails to mention how the joint regions were extracted in the first place [29]. Furthermore, an XGBoost model was trained to classify the severity of the OA.

2. Methodology

A pre-trained U-Net was employed for the detection of knee joints and subsequent segmentation of the femur and tibia bones in knee X-rays. The methodology is divided into two sections: the first section

focuses on detecting and extracting knee joints from X-ray images, while the second section concentrates on segmenting femur and tibia bones for JSW measurement.

2.1. Dataset

The images were obtained from the Osteoarthritis Initiative (OAI), a multi-center research study on knee health [30]. This study encompassed a cohort of 4,800 participants and recorded the development of knee osteoarthritis while concurrently tracking relevant biochemical biomarkers. It consisted of Bilateral radiographic anteroposterior (AP view) images of both men and women aged between 45 and 79. A collection of 103 bilateral radiographs was used for the purpose of joint detection and extraction. Subsequently, 276 joint images were employed specifically for bone segmentation procedures.

2.2. Pre-Processing

The original 16-bit (DICOM) bilateral X-rays were converted into '8-bit PNG' images to make them suitable for further processing. Due to variations in dimensions among the radiographs, manual cropping was performed to adjust them to 2048x2048 pixels. The images were cropped to preserve their aspect ratio and image quality. These cropped images were then used to generate square segmentation masks sized 512x512, positioned on top of the knee joints, as illustrated in Figure 1(b). The creation of segmentation masks was accomplished using an image annotation tool called CVAT (https://www.cvat.ai/).

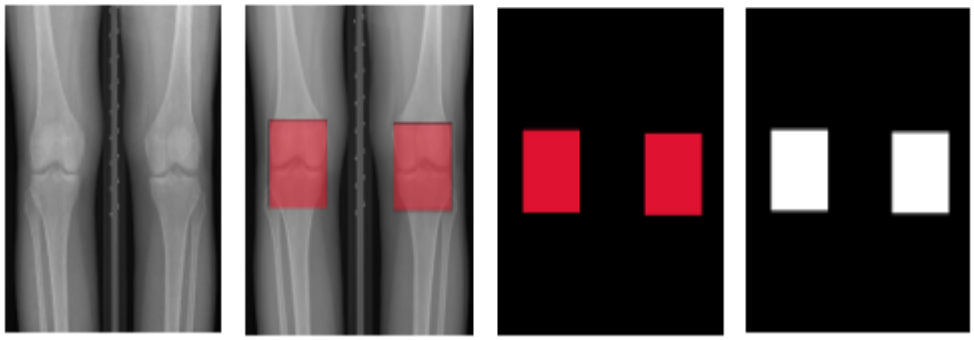

Figure 1. Shows the results of preprocessing operations. (a) Result of cropped image. (b) Shows the process of mask annotation. (c) Annotated mask; the red squares represent the joints. (d) Binary mask.

The masks were converted to binary, assigning a value of 0 to background pixels and a value of 255 to foreground pixels. The cropped images and their corresponding annotated masks were resized to 256x256 before feeding them into the network. The preprocessing results are illustrated in Figure 1.

2.3. Segmentation using U-NET

U-Net, a Convolutional Neural Network designed for biomedical image segmentation, was introduced in [31]. Its significant advantage lies in its ability to achieve robust performance with fewer training images compared to other models requiring thousands. U-Net operates on a pixel-based classification concept, assigning each pixel a class to generate a segmentation mask.

The basic U-Net architecture is composed of a contractive and an expensive path, also known as encoder and decoder respectively. The U-Net model used for segmentation, features a VGG11 encoder which is a CNN based model pretrained on ImageNet data, as proposed in [32]. The rationale behind using pretrained weights from a large dataset, as argued in [32], is to enhance performance when dealing with a small dataset, rather than training a model from scratch. The VGG11 architecture comprises of eleven sequential layers together with 7 convolutional layers, accompanied by a Rectified Linear Unit (ReLU) activation function and subsequent Max-Pooling operation as shown in Figure 2. The size of the kernels used in each of the convolutional layers is 3x3. The number of channels gradually increases from 64 in the initial layer to 512 just before the decoder block after each Mx-Pooling operation. In the U-Net structure, VGG11 served as the encoder by substituting the fully connected layers with a convolutional layer featuring 512 channels. The contracting path serves for down sampling feature maps while the expansive path serves for up-sampling feature maps. The decoder, responsible for image up-sampling, uses transposed 2D convolutions to enlarge feature maps and decrease channel numbers. Each transposed convolutional layer's result is combined with the corresponding encoder output.

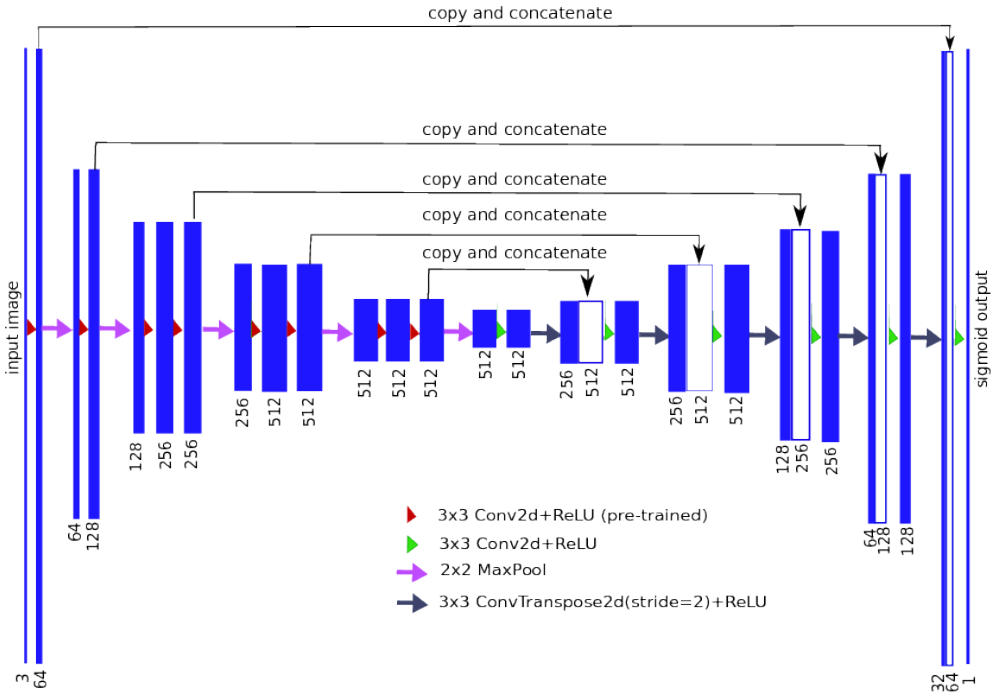

Figure 2. U-NET architecture (VGG11 as encoder)

2.4. Joint Detection using U-NET

For joint segmentation, the U-Net model underwent training using 83 bilateral X-ray images alongside their respective binary masks. The validation and test sets comprised 10 samples each. Augmentation pipelines were established for both training and validation to address the challenge of limited training samples. A "ShiftScaleRotate" transformation was applied, involving shifts, scales, and rotations with a probability of 0.5. The outcome of this augmentation was then subjected to "RGBShift", altering channel values with a shift limit of 25. Subsequently, "RandomBrightnessContrast" was employed to modify the brightness and contrast of the images.

Figure 3. Shows the results of mask annotation on knee joints. (a) Joint Image. (b) Shows the process of mask annotation. (c) Annotated mask. (d) Binary mask of knee joint.

The pixel values in the binary mask images ranged from 0 to 255, which were normalized to a range between 0 to 1. By using transfer learning, the pre-trained U-Net was utilized on knee images to categorize each pixel into the 0 or 1 class. Here, the value 0 represents the black background within the mask, whereas 1 indicates the white area depicting the joint bones. The pre-trained model underwent training on X-ray images for 8 epochs, employing a binary cross-entropy loss function. This process is illustrated in Figure 3.

2.5. Joint Extraction

The segmentation masks generated by the network were upscaled to their original size. Following this step, the images underwent a partitioning process, splitting them into two halves. This division aimed to discern between left and right knee images of the bilateral masks. The knee joint centers were determined by using Hu's moments which identified the contours within the white regions. Using these identified center points as references, the joint regions were cropped from the original images. This involved

extracting 256 rows both above and below the central row, as well as 256 columns to the left and right of the central column. As a result, all joint images shared the consistent dimensions of 512x512.

2.6. Bone Segmentation

Annotations were applied on the extracted joint images to produce segmentation masks that precisely outlined the femur and tibia bones, as depicted in Figure 4. Out of a set of 276 joint images, 241 were designated for training purposes, while 10 were utilized for validation, and the remaining 25 were allocated for testing the efficacy of the U-Net model. The image selection process was random. Due to the manual and time-consuming nature of mask creation, only 276 images were utilized for training.

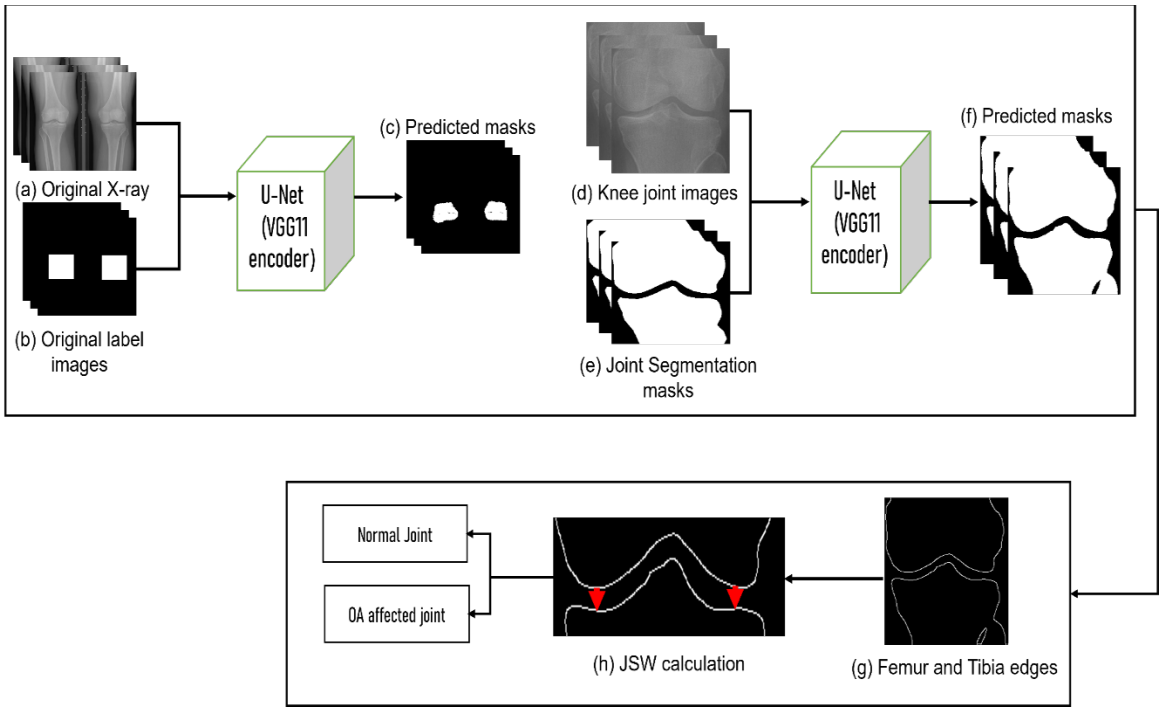

Figure 4. Shows the joint detection and bone segmentation process. (a) Bilateral X-ray images (b) Segmentation masks with white regions representing joints (c) Masks generated by the model (d) Knee joint images.
(e) Segmentation masks with white regions representing bones (f) Masks generated by the model for bone segmentation. (g) Result of edge detection. (h) Joint Space Width calculation.

Similar augmentation techniques, as mentioned earlier, were employed once again to improve segmentation results. The segmented joint images and their corresponding masks were introduced as input into the pretrained U-Net, as depicted in Figure 4(d) and 4(e). The network was trained for a total of 10 epochs utilizing a binary cross-entropy loss function. An Intersection Over Union (IOU) metric, or the Jaccard Index was used for evaluating the segmentation results. This metric quantifies the overlap between the target mask and the predicted mask. The IOU value ranges from 0 to 1, where 0 indicates no overlap and 1 signifies complete overlap between the target mask and the predicted mask as expressed in Equation 1.

$$Intersection\ Over\ Union\ (IOU) = \frac{target \cap prediction}{target \cup prediction} \quad (1)$$

2.7. Minimum JSW Segmentation

The predicted masks generated by the network were subjected to Canny edge detection to compute the boundaries outlining the joint bones. Within the medial compartments of the knee joints, the vertical distance between the end point of the femur boundary and the initiation point of the tibia boundary was calculated. The distance between the boundary pixels was calculated using the Euclidean distance metric, as defined in Equation 2.

$$Euclidean\ distance = d(p,q)\sqrt{\sum_{i=i}^{n}(q_i - p_i)^2} \quad (2)$$

Equal sets of boundary pixels were selected from the medial compartments of femur boundaries (edges), and the distances to their respective counterparts in the tibia boundaries were computed. The smallest distance, amongst all these calculated distances, was regarded as the minimum joint space width. The algorithm for vertical distance measurement was applied to 55 joint images, and the findings of this process are illustrated in Figure 5.

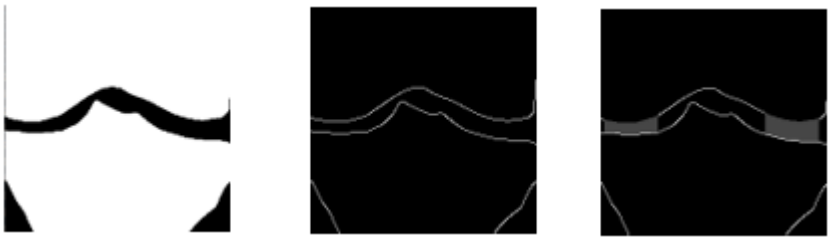

Figure 5. Demonstrates the process of distance measurement between femur and tibia edges. (a) Binary mask.
(b) Edges obtained after applying Canny edge operation. (c) Depicts detected edges with gray regions
representing the vertical distance in Medial and Lateral regions.

To accommodate the downscaling from the original joint image size of 512x512 pixels to the resolution of 256x256 pixels used during training, the minimum distance was doubled. This adjustment was made because the joint space width is measured in millimeters. To convert the pixel distance to millimeters, Equation 3 was employed, considering Pixels Per Inch (PPI), which indicates the number of pixels that fit into one inch of the screen. For this study, a screen PPI of 96 was assumed.

$$Minimum\ JSW\ in\ millimeters = \frac{(pixels * 25.4)}{PPI} \quad (3)$$

3. Results & Discussion

3.1. Performance Evaluation of Joint Detection & Segmentation

The first step in the proposed methodology involves joint detection, which is crucial to accurately locate knee joints for bone segmentation. The outcomes of joint detection are illustrated in Figure 6. The achieved mean Intersection Over Union (IOU) for joint segmentation stands at 0.588. Notwithstanding the relatively modest score, the algorithm demonstrated success in extracting all joint regions by precisely identifying the central points of the contours.

Figure 6. Shows the pixel classification and the mask generation process. (a) bilateral radiograph image.
(b) Binary mask with white regions indicating knee joints. (c) Binary mask predicted by the model.

3.2. Femur and Tibia Bone Segmentation Performance

The bone segmentation results for several normal knee joint images are presented in Figure 7. The mean Intersection Over Union (IOU) achieved for segmentation is 0.963. This result signifies highly promising segmentation outcomes, as evidenced by the high IOU score. An IOU of 0.963 indicates that there is a substantial overlap between the predicted segmentation masks and the ground truth masks, demonstrating the model's accuracy in accurately delineating the bone regions in the normal knee joint images. In essence, a higher IOU score closer to 1 indicates better agreement and alignment between the predicted

and actual segmentation, suggesting robust performance in accurately identifying and isolating the bone structures in the images.

Figure 7. Displays femur and tibia segmentation results. (a) Cropped knee joint. (b) Binary mask depicting bone boundaries. (c) Binary mask predicted by the model.

3.3. Classification of Osteoarthritis (OA)

The last phase within the algorithm distinguishes between a normal knee and an OA affected knee. Utilizing the minimum Joint Space Width (JSW) derived from the prior step alongside the Kellgren-Lawrence (KL) grades provided in the ground truth dataset forms the basis for this decision. The dataset only includes KL grades for the medial compartments in both the left and right knees, hence focusing solely on the readings of the medial compartment. As the dataset consists of KL grades for medial compartments in knee X-rays, only the readings of the medial compartments were taken into consideration.

Due to the manual creation of masks, the calculated minimum JSW readings were mapped to the KL grades. For all images with a minimum JSW less than 6.35mm, were classified as indicative of osteoarthritis, while readings equal to or greater than 6.35mm were categorized as healthy knee joints. A precise binary classification was achieved by matching these values with the KL grades in the dataset. The performance metrics of the distance calculation algorithm include an accuracy of 0.89, precision of 0.96, recall of 0.84, and specificity of 0.95. These metrics collectively demonstrate the algorithm's ability to effectively distinguish between normal and osteoarthritic knee joints, highlighting its accuracy, precision in positive predictions, ability to capture true positive cases, and capability to accurately identify true negative cases, respectively.

3.4. Discussion

Table 1 presents a comparative analysis of our proposed approach with existing solutions. The examination reveals that both [8] and our method have attained elevated mean Intersection Over Union (IOU) scores, indicating promising outcomes in bone segmentation. Nevertheless, it is notable that [8] lacks a detailed explanation of the process for extracting joint regions from bilateral X-ray images, a pivotal step in the context of knee radiographs. In contrast, our solution demonstrates success in precisely classifying joint images into normal and osteoarthritis-affected categories, achieving an accuracy rate of 89%. This indicates the effectiveness of our method not only in segmentation but also in the subsequent classification task, highlighting its comprehensive and robust performance.

Table 1. Comparison of the proposed method with State-of-the-Art Approaches

Author	Dataset	Joint Detection	Bone Segmentation	IOU	Classifier	Accuracy
Antony [20]	OAI, MOST	FCN	-	-	CNN	60.3%
Tiulpin [21]	OAI	Region Proposal Algorithm	-	-	Deep Siamese CNN	66.71%
P. Chen [26]	OAI	YOLOv2	-	-	VGG-19	69.7%
Cheung [29]	OAI	-	ResU-Net	0.98	JSW calculation	-
Our Approach	OAI	U-Net (VGG11 encoder)	U-Net (VGG11 encoder)	0.963	JSW calculation	89%

4. Conclusions

The primary objective of this study was to achieve accurate segmentation of femur and tibia bone regions from knee radiographs to measure the minimum Joint Space Width (JSW) between the bones, providing insights into the presence of osteoarthritis (OA) in the knee. In our proposed approach, we employed a deep learning model to autonomously segment joints from bilateral knee radiographs. Leveraging contour detection, the joints were precisely extracted from the original X-ray images. Additionally, the bones were segmented from the joints, and edge detection was employed to calculate the minimum JSW in all images through the development of a vertical distance measurement algorithm.

The recorded distance measurements were successfully classified into OA-affected or normal categories based on the ground truth dataset, which included Kellgren-Lawrence (KL) scores and joint space width measurements. The classification achieved an accuracy of 89%, indicating the effectiveness of our approach in distinguishing between OA-affected and normal knee joints.

Looking ahead, our future work will extend this research to perform a more comprehensive multi-class classification, encompassing KL grades 0 to 4. This expansion will further enhance the scope and applicability of our methodology in assessing different stages of knee osteoarthritis. In addition, the size of the dataset will be improved. The utilization of a small dataset was necessitated by the time-intensive mask creation process. Enhancing this process would enable the model to seamlessly handle broader range of knee radiographs.

Author Contributions: Conceptualization, A.K., and Z.S., methodology, A.K., Z.S. and M. A. A.; validation, M. A. A., and Z.S.; investigation, M.A.A, A.K., and A.A.; writing—original draft preparation, A.K., A.A., and Z.S, writing—review and editing, A.A., Z.Z., and A.K. All authors have read and agreed to the published version of the manuscript.
Conflicts of Interest: The authors declare no conflict of interest.

References

1. Ayaz, S.B., et al., The use of complementary health approaches among patients with knee osteoarthritis in Pakistan: A hospital based survey. The Egyptian Rheumatologist, 2016. 38(2): p. 111-116.
2. Vijayakumari, G. and G. Holi, Spatial Domain Approach for Articular Cartilage Segmentation of X-Ray Image. International Journal of Computer Applications. 975: p. 8887.
3. Felson, D.T., et al., The prevalence of knee osteoarthritis in the elderly. The Framingham Osteoarthritis Study. Arthritis & Rheumatism: Official Journal of the American College of Rheumatology, 1987. 30(8): p. 914-918.
4. Hunter, D.J., J.J. McDougall, and F.J. Keefe, The symptoms of osteoarthritis and the genesis of pain. Rheumatic Disease Clinics of North America, 2008. 34(3): p. 623-643.
5. Ozdemir, F., et al., How do marginal osteophytes, joint space narrowing and range of motion affect each other in patients with knee osteoarthritis. Rheumatology international, 2006. 26: p. 516-522.
6. Kohn MD, Sassoon AA, Fernando ND. Classifications in Brief: Kellgren-Lawrence Classification of Osteoarthritis. Clin Orthop Relat Res. 2016 Aug;474(8):1886-93. doi: 10.1007/s11999-016-4732-4. Epub 2016 Feb 12. PMID: 26872913; PMCID: PMC4925407.
7. Mengko, T.L., et al. Automated detection of unimpaired joint space for knee osteoarthritis assessment. in Proceedings of 7th International Workshop on Enterprise networking and Computing in Healthcare Industry, 2005. HEALTHCOM 2005. 2005. IEEE.
8. Oka, H., et al., Fully automatic quantification of knee osteoarthritis severity on plain radiographs. Osteoarthritis and Cartilage, 2008. 16(11): p. 1300-1306.
9. Gornale, S.S., P.U. Patravali, and R.R. Manza, Detection of osteoarthritis using knee x-ray image analyses: a machine vision based approach. Int. J. Comput. Appl, 2016. 145(1): p. 20-26.
10. Shamir, L., et al., Knee x-ray image analysis method for automated detection of osteoarthritis. IEEE Transactions on Biomedical Engineering, 2008. 56(2): p. 407-415.
11. Chen, H., et al. Automated segmentation for patella from lateral knee X-ray images. in 2009 Annual International Conference of the IEEE Engineering in Medicine and Biology Society. 2009. IEEE.
12. Jacob, N.E. and M. Wyawahare, Tibia bone segmentation in X-ray images-a comparative analysis. International Journal of Computer Applications, 2013. 76(9).
13. Cootes, T.F., et al., Active shape models-their training and application. Computer vision and image understanding, 1995. 61(1): p. 38-59.
14. Anu, T. and R. Raman, Detection of bone fracture using image processing methods. Int J Comput Appl, 2015. 975: p. 8887.
15. Kazeminia, S., et al. Bone extraction in X-ray images by analysis of line fluctuations. in 2015 IEEE International Conference on Image Processing (ICIP). 2015. IEEE.
16. Stolojescu-Crisan, C. and S. Holban. An Interactive X-Ray Image Segmentation Technique for Bone Extraction. in IWBBIO. 2014.
17. Tripathi, A.M., et al. Automatic detection of fracture in femur bones using image processing. in 2017 International Conference on Innovations in Information, Embedded and Communication Systems (ICIIECS). 2017. IEEE.
18. Umadevi, N. and S. Geethalakshmi, Enhanced Segmentation Method for bone structure and diaphysis extraction from x-ray images. International Journal of Computer Applications, 2012. 37(3): p. 30-36.
19. Vigil, M.A. and V.S. Bharathi, Detection of periodontal bone loss in mandibular area from dental panoramic radiograph using image processing techniques. Concurrency and Computation: Practice and Experience, 2021. 33(17): p. e6323.
20. Antony, J., et al. Automatic detection of knee joints and quantification of knee osteoarthritis severity using convolutional neural networks. in Machine Learning and Data Mining in Pattern Recognition: 13th International Conference, MLDM 2017, New York, NY, USA, July 15-20, 2017, Proceedings 13. 2017. Springer.
21. Tiulpin, A., et al., Automatic knee osteoarthritis diagnosis from plain radiographs: a deep learning-based approach. Scientific reports, 2018. 8(1): p. 1727.

22. Rebholz-schuhmann, D. and J. Newell, predicting knee osteoarthritis severity: comparative modeling based on patient's data and plain X-ray images. 2020.
23. Swiecicki, A., et al., Deep learning-based algorithm for assessment of knee osteoarthritis severity in radiographs matches performance of radiologists. Computers in biology and medicine, 2021. 133: p. 104334.
24. Thomas, K.A., et al., Automated classification of radiographic knee osteoarthritis severity using deep neural networks. Radiology: Artificial Intelligence, 2020. 2(2): p. e190065.
25. Wahyuningrum, R.T., et al. A new approach to classify knee osteoarthritis severity from radiographic images based on CNN-LSTM method. in 2019 IEEE 10th International Conference on Awareness Science and Technology (iCAST). 2019. IEEE.
26. Chen, P., et al., Fully automatic knee osteoarthritis severity grading using deep neural networks with a novel ordinal loss. Computerized Medical Imaging and Graphics, 2019. 75: p. 84-92.
27. Wang, Y., et al., An automatic knee osteoarthritis diagnosis method based on deep learning: data from the osteoarthritis initiative. Journal of Healthcare Engineering, 2021. 2021: p. 1-10.
28. Kwon, S.B., et al., Machine learning-based automatic classification of knee osteoarthritis severity using gait data and radiographic images. IEEE Access, 2020. 8: p. 120597-120603.
29. Cheung, J.C.-W., et al., Superiority of multiple-joint space width over minimum-joint space width approach in the machine learning for radiographic severity and knee osteoarthritis progression. Biology, 2021. 10(11): p. 1107. The Osteoarthritis Initiative
30. Ronneberger, O., P. Fischer, and T. Brox. U-net: Convolutional networks for biomedical image segmentation. in Medical Image Computing and Computer-Assisted Intervention–MICCAI 2015: 18th International Conference, Munich, Germany, October 5-9, 2015, Proceedings, Part III 18. 2015. Springer.
31. Iglovikov, V. and A. Shvets, Ternausnet: U-net with vgg11 encoder pre-trained on imagenet for image segmentation. arXiv preprint arXiv:1801.05746, 2018.